



OPEN ACCESS

EDITED BY

Francisco Rodriguez-valera,
Miguel Hernández University of Elche, Spain

REVIEWED BY

Yingwang Ye,
Hefei University of Technology, China
Cristobal Chaidez,
National Council of Science and Technology
(CONACYT), Mexico

*CORRESPONDENCE

Nela Nikolic
✉ nelanik@gmail.com
Fabrice Gielen
✉ f.gielen@exeter.ac.uk

RECEIVED 17 July 2023

ACCEPTED 23 October 2023

PUBLISHED 21 November 2023

CITATION

Nikolic N, Anagnostidis V, Tiwari A, Chait R and
Gielen F (2023) Droplet-based methodology
for investigating bacterial population dynamics
in response to phage exposure.
Front. Microbiol. 14:1260196.
doi: 10.3389/fmicb.2023.1260196

COPYRIGHT

© 2023 Nikolic, Anagnostidis, Tiwari, Chait and
Gielen. This is an open-access article
distributed under the terms of the [Creative
Commons Attribution License \(CC BY\)](#). The
use, distribution or reproduction in other
forums is permitted, provided the original
author(s) and the copyright owner(s) are
credited and that the original publication in this
journal is cited, in accordance with accepted
academic practice. No use, distribution or
reproduction is permitted which does not
comply with these terms.

Droplet-based methodology for investigating bacterial population dynamics in response to phage exposure

Nela Nikolic^{1,2,3*}, Vasileios Anagnostidis^{1,2}, Anuj Tiwari¹,
Remy Chait^{1,4} and Fabrice Gielen^{1,2*}

¹Living Systems Institute, Faculty of Health and Life Sciences, University of Exeter, Exeter, United Kingdom, ²Department of Physics and Astronomy, Faculty of Environment, Science and Economy, University of Exeter, Exeter, United Kingdom, ³Translational Research Exchange @ Exeter, University of Exeter, Exeter, United Kingdom, ⁴Department of Biosciences, Faculty of Health and Life Sciences, University of Exeter, Exeter, United Kingdom

An alarming rise in antimicrobial resistance worldwide has spurred efforts into the search for alternatives to antibiotic treatments. The use of bacteriophages, bacterial viruses harmless to humans, represents a promising approach with potential to treat bacterial infections (phage therapy). Recent advances in microscopy-based single-cell techniques have allowed researchers to develop new quantitative methodologies for assessing the interactions between bacteria and phages, especially the ability of phages to eradicate bacterial pathogen populations and to modulate growth of both commensal and pathogen populations. Here we combine droplet microfluidics with fluorescence time-lapse microscopy to characterize the growth and lysis dynamics of the bacterium *Escherichia coli* confined in droplets when challenged with phage. We investigated phages that promote lysis of infected *E. coli* cells, specifically, a phage species with DNA genome, T7 (*Escherichia virus T7*) and two phage species with RNA genomes, MS2 (*Emesvirus zinderi*) and Q β (*Qubevirus durum*). Our microfluidic trapping device generated and immobilized picoliter-sized droplets, enabling stable imaging of bacterial growth and lysis in a temperature-controlled setup. Temporal information on bacterial population size was recorded for up to 25 h, allowing us to determine growth rates of bacterial populations and helping us uncover the extent and speed of phage infection. In the long-term, the development of novel microfluidic single-cell and population-level approaches will expedite research towards fundamental understanding of the genetic and molecular basis of rapid phage-induced lysis and eco-evolutionary aspects of bacteria-phage dynamics, and ultimately help identify key factors influencing the success of phage therapy.

KEYWORDS

Escherichia coli, phage, bacterial population, bacterial growth, phage-induced lysis, phage therapy, droplet microfluidics, time-lapse microscopy

Introduction

Phages (bacterial viruses) are the most numerous biological entities, and their genomes consist of single- or double-stranded DNA or RNA. Seawater contains up to 10^7 DNA phage particles per milliliter (Henn et al., 2010), and sewage samples worldwide contain 10^2 – 10^7 RNA phage particles per milliliter (van Duin and Tsareva, 2006). The constant arms race between

bacteria and phages in nature produces complex coevolutionary dynamics, with emerging mechanisms that shape bacterial antiphage defense and phage counter-defense strategies (van Houte et al., 2016; Koskella et al., 2022). Phages therefore play important roles in the global ecosystem, continuously influencing microbial community dynamics and processes from biogeochemical cycling to human health.

As phages are natural killers of bacteria, they have been considered to be part of the antibacterial treatment, referred to as phage therapy, especially when designing treatments against infections caused by multi-drug resistant bacterial pathogens (Abedon, 2019; Kortright et al., 2019; Abedon et al., 2021; Iglar, 2022; Venturini et al., 2022; Maimaiti et al., 2023; Petrovic Fabijan et al., 2023; Strathdee et al., 2023). Phages are selective towards the bacterial host they infect, and usually narrowly target a single bacterial species or even a specific strain within the species. Phages are currently used as therapeutics for humans only in compassionate cases, however, phage therapy is already in veterinary use in livestock and other animals (McCallin et al., 2019). Even though phages can interact with host immune systems, they do not seem to trigger a strong immune response, and are thus far considered nontoxic to humans and animals (Nale and Clokie, 2021; Champagne-Jorgensen et al., 2023). Phage monotherapy and phage cocktail (a mixture of two or more phage species) are therefore promising alternatives for treating infections caused by clinically relevant bacterial pathogens where antibiotics are of no benefit or should even be completely avoided (Dedrick et al., 2019; Yang et al., 2020). Phages can also be administered in conjunction with conventional antibiotics, with several cases known where phage-antibiotic combinations eradicated infections more efficiently than the antibiotic alone (Suh et al., 2022; Van Nieuwenhuysse et al., 2022). Employing phage therapy as a novel clinical practice would require access to appropriate phage collections (Gibson et al., 2019; Maffei et al., 2021), and methodologies to rapidly determine the efficacy of phage-based treatments to eradicate pathogen populations and the likelihood of developing phage resistance.

Recent metagenomic studies have revealed novel phage sequences and substantially expanded their number in public databases, which subsequently led to restructuring of phage taxonomy (Lefkowitz et al., 2017; Walker et al., 2022). This shed light on phage genomic diversity, however without addressing their host range. Current bioinformatic methods fall short of predicting host range of phages solely from their genomics data and therefore cannot be used on their own (Zrellov et al., 2020). Instead, rapid and quantitative functional assays are required to evaluate phage infectivity and lytic activity against candidate bacterial hosts, especially clinical bacterial isolates. The standard plaque assays for phage enumeration and detection often involve demanding multistep protocols and long culturing times, and provide only limited throughput. On the other hand, high-throughput phage characterization can be performed but requires expensive and complex robotic systems (Chory et al., 2021).

Techniques able to obtain data at the single-cell level such as high-resolution microscopy will enable rapid screening of many microenvironments in parallel. In addition, time-lapse microscopy data can help gather extensive temporal information on bacteria-phage dynamics. This would therefore accelerate phage characterization procedures by quickly quantifying bacterial growth reduction and bacteriolysis at the single-cell level (Attrill et al., 2021; Nikolic et al., 2023).

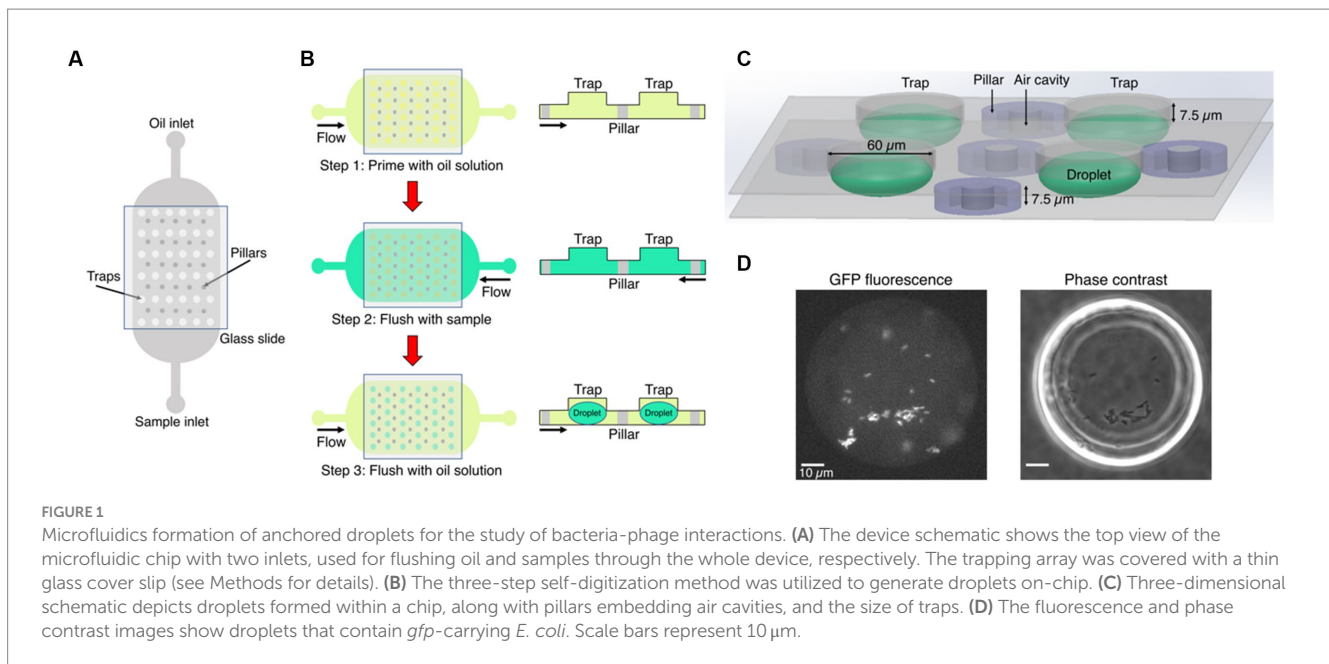
Current developments in combining microscopy with droplet microfluidic technologies have paved the way towards high-throughput quantitative analysis of living systems. Droplet technology enables controlled encapsulation of cells into water-in-oil microreactors (Matuła et al., 2020; Xu et al., 2020; Sun et al., 2023). Every reactor, typically of picoliter volume, represents a unique environment in which cells can proliferate. Droplet-based technology has to date been successfully applied to multiple research fields, including the directed evolution of enzymes or single-cell -omics protocols (Gielen et al., 2016, 2018; Anagnostidis et al., 2020; Gantz et al., 2023). Coupling of microfluidic-based systems with high-resolution microscopy enables a wide diversity of phenotypic screens, for instance cellular secretions, antibody production or the study of cell population growth (Liu et al., 2016; Kleine-Brüggeny et al., 2019; Rutkauskaite et al., 2022).

Several microfluidic-based microscopy setups have been successfully employed for monitoring fluorescently-labeled bacteria in droplets at the single-cell and population levels, using fluorescence signal as a proxy for number of bacterial cells or population size (Leung et al., 2012; Huang et al., 2015; Kaushik et al., 2017; Sabhachandani et al., 2017; Mahler et al., 2018; Postek et al., 2018; Barizien et al., 2019; Hsu et al., 2019; Pratt et al., 2019; Taylor et al., 2022). These studies have shown that microfluidic droplet technology can be used not only to quantify the growth of various bacterial species and microbial communities in different conditions, but also to test bacterial susceptibility to a range of antimicrobial compounds. In addition, droplet technology has been applied to develop phage detection and enumeration tools (Tjhung et al., 2014; Yu et al., 2014). However, these methods have not been adapted to study bacteria-phage interactions, and in particular have not explored whether lysis by phages can be successfully quantified from single-plane fluorescence maps. In our study, we developed a novel microfluidic device that generates anchored droplets populated with *E. coli* and their phage, with embedded air cavities used for precise autofocus. This collectively allowed for long-term evaluation of bacterial population dynamics across multiple droplets, enabling quantitative screening of phages as therapeutics to treat bacterial infections.

Materials and methods

Microfluidic device

Our microfluidic chips were fabricated using two-layer soft lithography processes (Figure 1A) (Bentley et al., 2022). Even though the chips contained one, two or three rows of traps located between rows of pillars, all traps had the same size and geometry (Supplementary Figure S1). The pillars contained square cavities filled with air during chip operation and used for the autofocus function. The height of the bottom flow channel was 7.5 μm . The top layer had circular traps of diameter of 60 μm and was 7.5 μm high, such that the overall height of the droplets was 15 μm . Uncured polydimethylsiloxane (PDMS) consisting of a 10:1 polymer to cross-linker mixture (Sylgard 184) was poured onto the master, degassed, and baked at 70°C for at least 4 h. Before this curing time at 70°C, a piece of 0.15 mm thick glass cover slip was immersed into the liquid PDMS and manually aligned above the trapping array. This method minimized droplet evaporation into the PDMS (Supplementary Figure S2). Following master mold



fabrication, PDMS chips were plasma bonded (Diener Zepto) on thin cover slip glass (thickness 0.15 mm) to enable high-resolution imaging. Hydrophobic surface treatment was performed after bonding by flushing with 1% (v/v) trichloro (1H,1H,2H,2H-perfluorooctyl) silane (Merck) in HFE-7500 and, subsequently, placed in a 65°C oven for 30 min.

Droplet generation

The microfluidic chip was placed on an epifluorescence microscope equipped with an automated stage. A self-digitization water-in-oil emulsion method was followed to make droplets (Figure 1B). First, the entire microfluidic chip was manually primed with a fluorinated oil (HFE-7500, Fluorochem Ltd.) solution supplemented with 1% w/w fluorosurfactant (008, RAN Biotechnologies) using a syringe. The main reason for using a surfactant in the oil solution is to reduce the interfacial tension between the sample and the oil phase. This facilitates the digitization process and prevents droplet coalescence (Cohen et al., 2010). The sample containing either bacteria or bacteria-phage mixture was then flushed through the chip using the opposite inlet to replace the HFE oil solution. The oil solution was subsequently flushed again through the chip forming droplets of volume 28 picoliters (assuming elliptical spheres).

Fluorescence time-lapse microscopy

Time-lapse imaging data were acquired using a temperature-incubated, μ Manager-controlled Olympus IX83 fluorescence microscope equipped with an LED light source (Lumencor SpectraX) and an automated stage (Marzhauser) (Edelstein et al., 2014; Chait et al., 2017). The incubation box (cellVivo) temperature was maintained at 30°C for all assays. Fluorescence and phase contrast images were acquired with an sCMOS camera (Hamamatsu Orca

Flash4v3) every 3 min through a 40 \times objective (UPLFLN40XPH, Evident Olympus). Up to six positions were recorded in each time-lapse, capturing four to six droplets per field of view. Air cavities in pillars of the microfluidic chip aided software-based autofocus (on 640 nm reflection images) performed prior to acquiring each image set (Figure 1C), as described in Chait et al. (2017). We then recorded a phase contrast image to confirm that traps are populated with sample-containing droplets, and a GFP fluorescence image (to quantify fluorescence-based population size) at a focal plane mid-way through the droplets at each position (Figure 1D). We set exposure time to 20 ms for phase images, and 100 ms was the exposure time to image GFP (excitation 460–480 nm, emission 495–540 nm, dichroic mirror 490 nm).

Image analysis

Raw fluorescence images were divided by a shading corrector image to account for inhomogeneity of GFP excitation illumination across the field of view, as described in (Chait et al., 2017). To obtain the shading corrector, we took a median projection through a stack of GFP images from distinct locations on a glass cover slip overlaid with 50% (w/v) fluorescein (Model and Burkhardt, 2001). We then normalized this corrector image by dividing by its median pixel value. After shading correction, we performed background subtraction by using “mask” images. Masks were made by finding the thresholds in each frame for which the background fluorescence value, i.e., signal not coming from fluorescent cells within droplets, corresponded to 0. Then, each shading-corrected image was multiplied with the respective mask image for each recorded frame. This final image was used to set a circular region of interest (ROI) around each droplet. We extracted mean fluorescence intensity per ROI corresponding to mean droplet fluorescence intensity. For the analysis, we excluded frames in which the device was out of focus. All image analysis routines were done in the open-source image

processing package Fiji (ImageJ) (Schindelin et al., 2012), and more details can be found in [Supplementary Methods](#).

Phages, strains and cultivation

One phage species with DNA genome, T7 (*Escherichia virus T7*) and two phage species with RNA genomes, MS2 (*Emesvirus zinderi*) and Q β (*Qubevirus durum*) were used in this study, together with *E. coli* strains BW25113, W1485, and the derivatives of K-12 MG1655 harboring the constitutively expressed *gfp* reporter gene encoding for Superfolder GFP, with strain genotypes described in [Supplementary Table S1](#). The F plasmid from strain W1485 was introduced by conjugation into strain TB193, now annotated as strain TB193 F+. Only strains that harbor the F plasmid can be infected by MS2 and Q β , as RNA phage start infection by adsorbing to bacterial F-pili encoded on the F plasmid. Phage T7 can infect all listed *E. coli* strains. Bacterial cultures were grown in LB medium (1% tryptone, 0.5% yeast extract, 1% NaCl), which is a nutrient-rich medium. Frozen glycerol clones were streaked on LB agar plates to obtain single colonies. A single colony was used to inoculate overnight batch cultures shaking at 230 rpm. All overnight incubations and batch cultivations prior to phage infection were carried at 37°C. Bacterial cultures were supplemented with 0.01% glucose and 2 mM CaCl₂ prior to adding RNA phage for infection experiments [addition of divalent ions facilitates phage adsorption (Rappaport, 1965, Ács et al., 2020)]. LB medium was supplemented with 10 µg/mL chloramphenicol for selection after conjugation.

Sample preparation for droplet assays

Overnight cultures of an *E. coli* strain were diluted 1 to 100 into 4 mL of fresh LB medium for 3 h at 37°C, to obtain exponentially growing cultures at $\sim 5 \times 10^8$ bacterial cells/mL. Bacterial cultures were then supplemented with 0.01% glucose and 2 mM CaCl₂. For phage infection experiments, aliquots of bacterial cultures were mixed with phage lysate of the known titer in a 1.5 mL-tube, yielding a specific multiplicity of infection (MOI, the ratio of phage particles to bacterial cells in a mixed culture), prior loading the sample into the microfluidic device. The exact time from preparing bacteria-phage mixture to starting the time-lapse microscopy experiment was noted (typically, 11–14 min). An additional aliquot of the bacterial culture was taken just before starting the microscopy experiment (or in the case of infection experiments, just before adding phage) to determine the initial bacterial population size. Serial dilutions of the culture aliquot were plated on LB agar plates and incubated at 37°C for 24 h. Bacterial population size was determined by measuring the density of colony forming units CFU, as: $\text{CFU/mL} = n_{\text{colonies}} / (\text{dilution factor} \times V_{\text{diluted culture}})$, and these measurements are included in [Supplementary Datasets](#). MOI values reported in figure legends were calculated based on the measured population size of each bacterial culture prior infection. As bacteria-phage mixtures were prepared prior droplet generation, the analyzed droplets had the same initial MOI in each experiment. We do expect some fluctuation in absolute initial phage numbers from Poisson statistics (Collins et al., 2015) but

this arguably becomes less significant following the first lysis event after which the number of phages in droplets would increase dramatically, as the reported phage burst sizes are in the range: 179–182 phage T7 particles/cell (Nguyen and Kang, 2014; Xu et al., 2021), 2,000–2,100 phage MS2 particles/cell (Rappaport, 1965; Jenkins et al., 1974), 90–776 phage Q β particles/cell (Woody and Cliver, 1995; Tsukada et al., 2009).

Phage lysate preparation

Overnight bacterial cultures of the *E. coli* host propagation strain (BW25113 for phage T7, W1485 for phages MS2 and Q β) were diluted 1 to 100 into LB medium. After 4 h, exponentially growing cultures were inoculated with a single plaque in 4 mL of phage soft agar (1% tryptone, 0.1% yeast extract, 0.01% glucose, 0.8% NaCl, 2 mM CaCl₂, 0.7% agar; kept at 50°C), plated on phage plates (1% tryptone, 0.1% yeast extract, 0.01% glucose, 0.8% NaCl, 2 mM CaCl₂, 1% agar), and incubated overnight at 37°C for 20 h (Nikolic et al., 2023). The following day, soft agar containing plaques was removed into a 50 mL-Falcon tube with 12 mL of SM buffer (0.1 M NaCl, 8 mM MgSO₄·7H₂O, 50 mM Tris-HCl pH 7.5, 0.01% gelatin). Falcon tubes were centrifuged for 15 min at 4,000 g. The supernatant containing phage lysate was filtered twice through a 0.22 µm-filter into a new tube. Phage lysates were kept at 4°C, and their phage titer was determined by plaque spotting assays described below.

Plaque spotting assays

Overnight cultures of the *E. coli* host strain were diluted 1 to 1,000 into LB medium. After 5.5 h, 200 µL of exponentially growing bacterial cultures were added to 4 mL of phage soft agar, and plated on phage plates (Nikolic et al., 2023). After 2–3 min, serial dilutions of the phage lysate were spotted on top of the soft agar containing bacterial host, and the plates were incubated overnight for 20 h, at 37°C for phages MS2 and Q β , or at room temperature for phage T7. Phage titer was determined by measuring the density of plaque-forming units PFU, as: $\text{PFU/mL} = n_{\text{plaques}} / (\text{dilution factor} \times V_{\text{diluted phage}})$.

Plate-reader experiments

Overnight *E. coli* cultures were diluted 1 to 100 into LB medium. After 3 h of cultivation, the cultures were supplemented with 0.01% glucose and 2 mM CaCl₂. Aliquots of the cultures were put into wells of a 96-well microplate, and each well was either infected with phage at the specific MOI, or the same volume of SM buffer was added to uninfected cultures. All samples were then diluted 1 to 10 into fresh LB medium, having final volume of 180 µL in each well. Four independent replicate cultures were analyzed in experiments with phage T7, and five independent replicates were analyzed in infection experiments with MS2 and Q β . Growth of the cultures was recorded at 30°C, every 4 min for 800 min in total, as absorbance at 600 nm A₆₀₀, with shaking prior to each measurement (CLARIOstar Plate Reader, BMG Labtech).

Analysis of growth and lysis

For each growth curve, we employed the Microsoft Excel function *slope* from ln-transformed measurements over a sliding window of 40 min, i.e., over 11 time points in plate-reader assays or 14 time points in droplet assays. Bacterial growth rate μ was then defined as the maximum slope value for each growth curve, within the period $t = 36\text{--}120$ min for droplet experiments, and $t = 20\text{--}120$ min for plate-reader assays. In addition, growth rates μ of bacterial populations challenged with RNA phage were determined within the period $t = 38\text{--}200$ min for droplet experiments, and $t = 24\text{--}200$ min for plate-reader assays. Doubling times (plate-reader assays) or fluorescence-based doubling times (droplet assays) corresponded to $\ln 2/\mu$. To mark the transition from initial bacterial growth to the onset of bacteriolysis, inflection points were evaluated for each growth curve from slopes calculated over a sliding window of 40 min, by identifying the time point where slope value changed from positive to negative. The middle time point of the sliding window was noted to be the inflection point. To evaluate differences between different conditions or different strains we used two-tailed two-sample heteroscedastic student's *t*-tests.

Results

Adapting droplet technologies for phage assays

We optimized the layout of a microfluidic device for easy self-digitization, enabling formation of stable droplet-environments and steady microscopy imaging routine. The microfluidic chip utilized in our experiments had two inlets, one for the oil phase and the other one for the aqueous samples, with a central large trapping chamber embedding dozens of traps and pillars (Figure 1A). A glass cover slip was immersed in the uncured PDMS and cured in place on top of the trapping area to minimize droplet evaporation and ensure the stability of droplets during the course of time-lapse experiments (Supplementary Figure S2). The chip was placed on an automated fluorescence microscopy imaging platform in an enclosed environmental box set to 30°C. We employed a three-step process to generate droplets on-chip following the self-digitization emulsion method, which means that emulsions were formed by consecutive flowing of aqueous and oil phases into the same chip (Figure 1B). In our study, the aqueous phase was the sample of either a sole bacterial culture, or a mixture of phage and susceptible bacteria cultivated in growth medium. The chips were first primed with the solution of oil containing surfactant, and the sample was then flushed through the chip using the opposite inlet so that the sample could fill all traps. The oil solution was then flushed again and droplets were passively formed within the traps. Interfacial tension and density difference between aqueous samples and oil generated anchored droplets that had the diameter of the designed traps (Supplementary Figure S1). In our experiments, droplets were formed in 96% of traps within the field of view, while the remaining 4% were either empty traps or traps populated with more than one droplet (Supplementary Datasets). Moreover, each microfluidic chip consisted of rows of traps followed by rows of pillars (Figure 1C). Air cavities were included at the center of pillars to identify them and provide fiducials at the glass interface

to aid software-based autofocusing performed using 640 nm illumination prior to imaging at each time point and location (Chait et al., 2017) (Supplementary Figure S1). Stable autofocusing enabled steady image acquisition from several pre-selected positions on the chip per each time point, and ensured reproducible imaging despite microscope stage motion (Figure 1D). The small height of the chamber (15 μm) ensured accurate quantification of overall fluorescence produced by the cells. Finally, we utilized a rapid and simple image analysis routine from the widely-used open-source image analysis software platform Fiji (ImageJ) to quantify mean fluorescence intensity of each droplet (see Supplementary Methods). Altogether, we developed a device and workflow for the on-chip droplet generation and stable multidroplet microscopy image acquisition dedicated to the long-term monitoring of bacterial growth and lysis in droplets.

Evaluating the efficacy of phage-induced lysis in droplets

We first assessed how droplet-environments support the growth of *Escherichia coli* carrying chromosomally encoded, constitutively expressed *superfolder gfp*. An exponentially growing *E. coli* culture was loaded into a primed microfluidic device subsequently flushed with oil to form bacteria containing-droplets within traps. We monitored the increase in GFP fluorescence coming specifically from all cells during the time-lapse microscopy experiment, as the proxy for bacterial population growth in droplets. Despite known stochastic fluctuations in *gfp* expression in clonal bacterial populations, a broadly linear correlation between integrated droplet fluorescence and the number of fluorescent bacterial cells in droplets has been reported previously (Barizien et al., 2019; Taylor et al., 2022). For this and all subsequent droplet experiments, we aimed at loading 10 to 40 bacterial cells in each droplet, with the number of bacterial cells across droplets following a Poisson distribution, as previously established in Collins et al. (2015) and Taylor et al. (2022). We measured a mean 30-fold GFP fluorescence increase of the droplet populations over 400 min of the time-lapse experiment (Figure 2A, Supplementary Movie S1). Our analysis showed that the mean fluorescence-based doubling time of bacterial populations in droplets was 24 ± 8 min (mean \pm standard deviation). The mean doubling time of the same strain growing in a plate-reader was 34 ± 2 min (Figure 2B). Overall, our results indicate that *E. coli* populations can successfully grow inside droplet-environments within designed microfluidic devices, with a growth pattern comparable to bulk batch cultures.

Next, we investigated whether we can utilize the same droplet-based setup to monitor the dynamics of bacterial populations challenged with phages. To this end, we mixed bacterial cultures of *gfp*-carrying *E. coli* with phage lysate prior to loading the sample into a microfluidic device. In all our experiments, we employed obligatory lytic phages, which are phages that promote bacteriolysis and kill infected bacterial cells. Subsequently, decline in bacterial population size due to lysis of bacterial cells, i.e., the biomass reduction within droplets, was detected as a decrease in overall GFP fluorescence. In the first set of experiments, we infected *E. coli* cultures with phage T7 at MOI ~ 1 . T7 is a phage species with DNA genome, and is known for its short replication cycle (time from infection to the lysis of the host cell) of typically 15 min at 37°C, and 30 min at 30°C, and

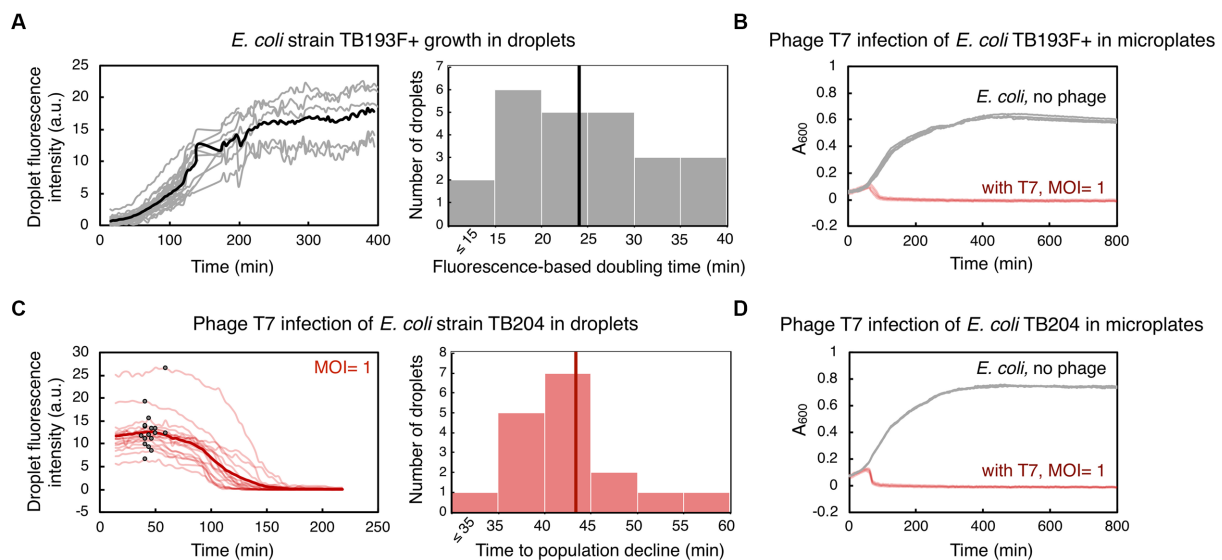


FIGURE 2

Bacterial growth and phage T7-induced bacterial population decline in droplets and in microplates. (A) An exponentially growing culture of *E. coli* strain TB193 F+ harboring the *gfp* fluorescent reporter gene was loaded into a microfluidic device at 2.2×10^8 CFU/mL (CFU, colony forming unit). GFP fluorescence intensity over time for 24 individual droplets is plotted in gray, and the black line is the mean value over all GFP fluorescence trajectories. The GFP signal of all droplets was collected for at least 120 min, and five individual droplets were followed until 400 min (see [Supplementary Methods](#) and [Supplementary Datasets](#)). The histogram shows the distribution of fluorescence-based doubling times of *E. coli* droplet populations growing in nutrient-rich medium, with the mean doubling time of 24 min (black line). (B) Population size of TB193 F+ cultures, either infected with phage T7 or uninfected, was monitored in a plate-reader by recording absorbance at 600 nm (A_{600}). Phage T7 was added to the cultures at time 0 and multiplicity of infection, MOI = 1 (4 independent replicate cultures, light red lines), or no phage was added (4 replicates, gray lines). (C) *E. coli* strain TB204 harboring the *gfp* fluorescent reporter gene (6.3×10^8 CFU/mL) was mixed with phage T7, at MOI = 1. Temporal information for GFP fluorescence intensity of 17 individual droplets is plotted in light red, and the thick red line is the mean value over all droplets. We determined the inflection point for each trajectory corresponding to the start of bacteriolysis in each droplet, i.e., the time point after which the bacterial droplet population size declines (indicated as black dots on light red lines). The histogram shows the distribution of times to population size decline, with the mean time of 43 min (thick red line). (D) Population growth and lysis assays of *E. coli* strain TB204 were performed in a plate-reader, with 4 uninfected and 4 infected independent replicate cultures.

a high efficacy in killing *E. coli* cells (Jack et al., 2019; Xu et al., 2021). By measuring GFP fluorescence, we detected a severe reduction in the *E. coli* population size during T7 infection in droplets. Our analysis indicated that on average 99.4% of an *E. coli* droplet population was killed 218 min after adding T7 phage (Figure 2C), with 0–2 cells per droplet remaining at the end of the time-lapse experiment (Supplementary Movies S2, S3). We determined the time point when infected bacteria in droplets had a population dynamics shifting from dominant growth to dominant lysis, by finding the inflection point of GFP fluorescence curves. The mean time to the population decline, i.e., to the start of significant bacteriolysis of droplet populations, was 43 ± 7 min. Growth and lysis assays in a plate-reader showed that the mean time to population decline during T7 infection was 46 ± 2 min, with the eradication of bacterial cultures, i.e., >99.9% of the population killed, happening after 165 ± 92 min (Figure 2D). In addition, time to T7-induced bacteriolysis was not significantly dependent on the presence of the *gfp* reporter gene in the *E. coli* genome (Supplementary Figure S3). The presence of the F plasmid slightly increased the time to lysis, by 19% on average, without significantly affecting the time to whole population eradication (Supplementary Figure S3 and Supplementary Table S2). Overall, these experiments suggest that droplet-based technology can be utilized to analyze bacterial population growth dynamics in response to phage, and to quantify the efficacy of phages to kill bacterial populations.

Investigating long-term dynamics between bacteria and phages

We evaluated the ability of generally poorly characterized phages with RNA genomes to influence the growth of *E. coli* populations in droplets. MS2 (*Emesvirus zinderi*) and Q β (*Qubevirus durum*) are the best known RNA phages, with longer phage replication cycle (typically 90 and 105 min at 37°C, respectively), different lysis machinery, and lesser efficacy in killing *E. coli* than DNA phage T7 (Rappaport, 1965; Jenkins et al., 1974; Woody and Cliver, 1995; Bernhardt et al., 2002; Tsukada et al., 2009; Nikolic et al., 2023). *E. coli* were mixed with RNA phage lysates at MOI ~ 10 , to ensure a large excess of phage particles and therefore an increased likelihood of infection; specifically, MS2 lysate at MOI = 7, and Q β lysate at MOI = 14. Droplets populated with bacteria-phage samples were then generated and trapped within a microfluidic device. Phage MS2 impeded bacterial growth in droplets, with fluorescence-based doubling time of droplet populations increasing more than 3-fold compared to uninfected populations, to 81 ± 16 min (Figure 3A, Supplementary Movie S4). Analysis of inflection points from GFP fluorescence curves indicated that droplet population size started to decline 374 ± 72 min after *E. coli* being challenged with MS2, in 63% of analyzed droplets. The remaining droplet populations either exhibited a reduced growth rate without population size

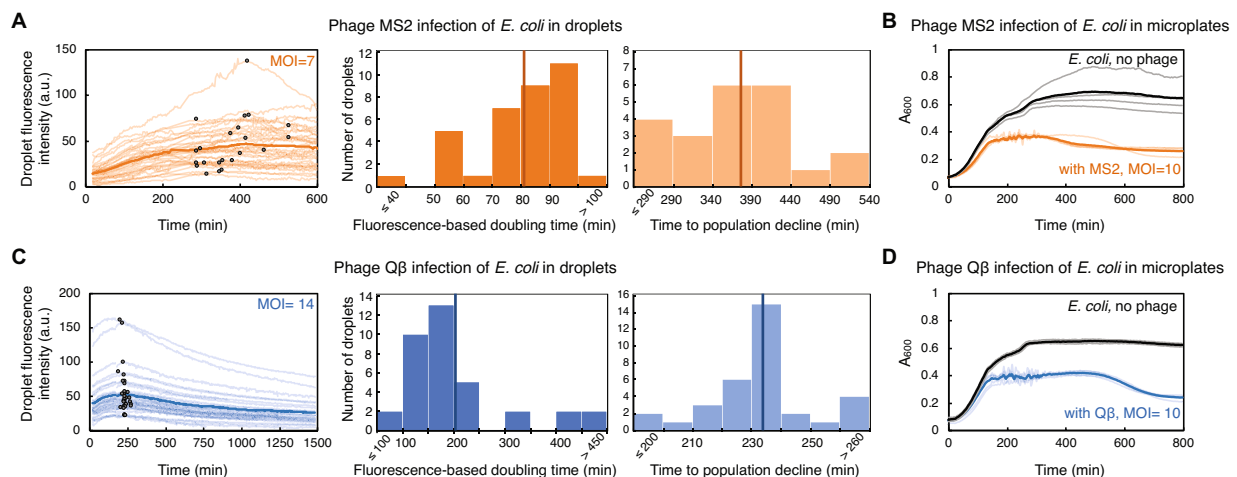


FIGURE 3

E. coli challenged with RNA phage in droplets and in microplates. (A) *E. coli* strain TB193 F+ (5.9×10^8 CFU/mL) was challenged with phage MS2, at MOI = 7. GFP fluorescence intensity of 35 individual droplets during MS2 exposure is plotted in bright orange (with inflection points depicted with black dots), and the dark orange line is the mean value across all droplets. The left histogram shows the distribution of fluorescence-based doubling times, which were estimated from the growth rates calculated during the first 200 min of the experiment. The mean value of 81 min is depicted with a dark orange line. The right histogram shows the distribution of times to the droplet population decline upon MS2 phage infection, inferred from inflection points of GFP fluorescence curves of 22 droplets, with the mean value of 374 min. (B) The same *E. coli* strain was mixed with phage MS2 at MOI = 10, and bacterial growth and lysis were monitored in a plate-reader. Light orange depicts lysis curves of 5 independent replicates, with the mean value across all replicates depicted in dark orange. Growth curves of 4 uninfected replicate cultures are depicted in gray, with the mean value across all replicates depicted in black. (C) *E. coli* culture (7.2×10^8 CFU/mL) was challenged with phage Q β , at MOI = 14. GFP fluorescence intensity recorded for 36 individual droplets during Q β exposure is plotted in light blue (with inflection points indicated as black dots), and blue line is the mean value across all droplets. The left histogram shows the distribution of fluorescence-based doubling times, with the mean value of 204 min depicted with dark blue line. The right histogram shows the distribution of times to the droplet-population decline upon Q β infection, inferred from inflection points of GFP fluorescence curves of 34 droplets, with the mean value of 233 min. (D) The growth dynamics of *E. coli* challenged with phage Q β at MOI = 10 was recorded in a plate-reader. Light blue presents lysis curves of 5 infected independent replicate cultures, with the mean value across all replicates shown in blue. Growth curves of 3 uninfected replicate cultures are depicted in gray, with the mean value depicted in black.

decline, or resumed growth shortly after the initial population size decline (Supplementary Datasets). Overall, after 601 min of exposure to phage MS2, we measured a mean 2.8-fold GFP fluorescence increase of the droplet populations compared to the GFP fluorescence intensity at the beginning of the experiment. This increase in the fluorescence level suggests that a subpopulation of the infected droplet population continued growing in the presence of phage MS2. Recent single-cell studies have indeed indicated heterogeneity in the bacterial response to phage exposure: some cells within the infected bacterial population lysed, some cells entered a dormant, non-dividing state, and some cells continued growing and dividing with different elongation rates (Attrill et al., 2021; Nikolic et al., 2023). In addition, we measured the growth dynamics of the same *E. coli* strain challenged with phage MS2 at MOI = 10 in a plate-reader (Figure 3B). The population doubling time in a plate-reader was 46 ± 4 min during MS2 exposure, and the size of all plate-reader populations started to decrease 310 ± 45 min after adding phage MS2.

Furthermore, we detected a reduction in bacterial growth after challenging *E. coli* with phage Q β , with the fluorescence-based doubling time of 204 ± 110 min for infected populations in droplets (Figure 3C, Supplementary Movie S5). The start of decline of the droplet population size was detected 233 ± 18 min after adding phage Q β , in 94% of analyzed droplets. At the end of the time-lapse experiment involving 1,481 min of exposure to phage Q β , we measured a mean 1.6-fold GFP fluorescence-decrease of the

droplet populations. Similarly to the experiments with phage MS2, we measured growth dynamics of *E. coli* populations challenged with phage Q β at MOI = 10 in a plate-reader (Figure 3D). The population doubling time during Q β exposure was 43 ± 3 min, and decline in the size of all plate-reader populations was noticed 445 ± 17 min after *E. coli* being challenged with phage Q β . Altogether, comparable phage-modulated bacterial growth dynamics between plate-reader and droplet experiments paves the way towards development of high-throughput multidroplet screening methods that can make bacteria-phage interaction analyses faster than standard microbiology methods.

In addition, the droplet experiment involving almost 25 h of phage exposure (Figure 3C) allowed us to test feasibility of the microscopy setup to monitor long-term bacteria-phage dynamics, which would be crucial for understanding underlying eco-evolutionary principles. Long-term exposure of bacteria to phages can generally lead to complex coevolutionary dynamics, with emerging bacterial antiphage resistance mechanisms as well as phage adaptation mechanisms facilitating more efficient infection of the host (van Houte et al., 2016; Koskella et al., 2022). In some of our experiments, we observed bacterial growth recovery during prolonged phage challenge, possibly due to mutations arising in bacterial genomes in the infected cultures, leading to antiphage resistance (Supplementary Figure S4). In conclusion, our findings indicate that utilizing droplet-based technology can provide quantitative temporal information on how phages modulate bacterial growth rate and alter population size of their bacterial host over longer periods of time.

Discussion

We have established a novel methodology that couples droplet-based assays in a microfluidic device to time-lapse fluorescence microscopy for studying bacteria-phage interactions and dynamics at population-level resolution. The described droplet generation technique eliminates the need for complex and expensive equipment (e.g., pumps), making it an accessible and cost-effective method for generating and monitoring droplets on-chip. Furthermore, our methodology delivers a unique approach to detect changes in bacterial population size upon phage infection, in a temperature-controlled environment, ensuring the stability of droplets and steady image acquisition over long time periods. For the image analysis pipeline, we employed a set of basic tools freely available from an open-source platform, without implementing any additional custom-made scripts or closed-source software packages. We successfully quantified the speed (time to bacteriolysis) and extent of invasion (fraction of the lysed bacterial population and the bacterial growth reduction) from three different phage species attacking a common bacterial species (Figure 4). As such, this methodology has a great potential to allow us to routinely assess both phages that can be effective pathogen-killers and phages that can modulate the structure of host-associated commensal bacterial populations.

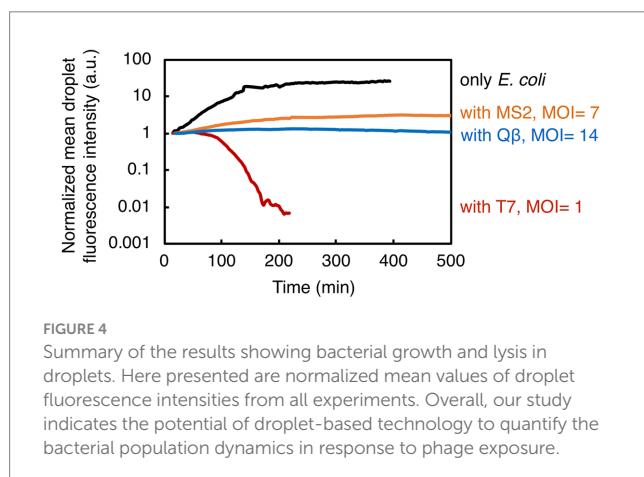
Overall, the specific advantage of having droplet-based assays at the population-level resolution is the ability to replicate batch cultures at the picoliter scale, and to resolve possible autoaggregation [formation of bacterial clumps (Trunk et al., 2018)] and dispersal events (detachment of cells from aggregates), as aggregate formation can often result in an inaccurate quantification of bacterial population size in microplates. Results of the droplet experiments were comparable to results of the plate-reader experiments, despite these two setups providing different environmental conditions, with the absence of shaking and limited oxygen diffusion in droplet environments (Huang et al., 2015).

Our high-resolution imaging modality enabled quantification of fluorescence signals down to single-cell resolution provided cell numbers were low and cells were in, or close to, optimum focus. Even though some cells were out-of-focus, they still contributed to the final mean fluorescence intensity readout provided their GFP signal was

above a threshold value (see Methods and Supplementary Methods). This issue was also mitigated by cell motility, which ensured consistent number of cells found in and out of focus across the time series. In addition, a stable autofocus function enabled reproducible focusing at a plane corresponding approximately to the middle of the droplet, over the experiment duration. The correct function is seen primarily through the smooth fluorescence-based growth and lysis curves that indicate that, despite mechanical motion of the microscope stage, images were acquired at a consistent focus throughout all the droplets screened. On the whole, absolute quantification of cell number was prevented mainly by autoaggregation and the presence of cells far from the focal plane. We note that large aggregates were mainly static and thus had consistent signals throughout (Supplementary Movie S5).

The established droplet-based methodology could be employed to fully unveil the potential of phages as therapeutics against bacterial diseases. Bacterial infections were the second leading cause of death globally prior the COVID pandemic (Ikuta et al., 2022). According to the World Health Organization, over 50% of life-threatening bacterial infections are caused by pathogens resistant to one or more antibiotics, with *E. coli* being the leading antibiotic-resistant pathogen responsible for the most deaths in 2019 (WHO, 2019; Ikuta et al., 2022; Murray et al., 2022). In particular, *E. coli* pathogenic strains involved in urinary tract infection (UTI) and food poisoning are major public health concerns worldwide. Antibiotic treatments are typically prescribed against UTIs, however *E. coli* can be found in the patient urinary tract weeks after antibiotic treatment, increasing the chance of relapse and chronic infections (Klein and Hultgren, 2020). UTI is the source for more than 50% of bloodstream infection (bacteremia) cases, and over 40% of the UTI-causing strains are resistant to some of the antimicrobials commonly used (Allocati et al., 2013; Bonten et al., 2021; McCowan et al., 2022; Murray et al., 2022; UK Health Security Agency, 2022). Antibiotic treatments against foodborne pathogens, Shiga toxin-producing *E. coli* strains are usually not recommended because the antibiotic-induced bacterial SOS response increases the Shiga toxin production and release, which damages host cells and can lead to severe disease outcomes (Mühlen and Dersch, 2020). A high-throughput bacteriolysis droplet screening platform that is able to quantify the heterogeneity, speed and extent of phage invasion could therefore be successfully employed when designing phage therapy against infections caused by multi-drug resistant or toxin-producing bacterial pathogens.

Various droplet-based platforms have been used for systematically testing antibiotic susceptibility of *E. coli* and other clinically relevant bacterial strains (Huang et al., 2015; Kaushik et al., 2017; Sabhachandani et al., 2017; Postek et al., 2018). Further droplet technology applications could include high-throughput screening of gene knockout libraries of bacterial strains to identify mechanisms underlying antibiotic action in bacterial cells (e.g., bacterial SOS response activated by DNA damage during antibiotic treatment). As combination phage-antibiotic treatments have been considered the most efficient type of phage therapy (Suh et al., 2022; Van Nieuwenhuysse et al., 2022), droplet-based screening platforms could be employed to better understand phage-antibiotic interactions and to identify mechanisms that drive those interactions. In addition, such platforms could implement the existing droplet digital PCR (ddPCR) technology, to understand molecular alongside cellular aspects of bacteria-phage dynamics (Morella et al., 2018; Spilsberg et al., 2021). ddPCR could quantify



DNA phage or RNA phage densities over time (by measuring their DNA or RNA content respectively), and also quantify bacterial and DNA phage densities simultaneously. Even though it has been reported that this technique can detect both non-infectious and infectious phage particles thus not necessarily informing on actual infection events, ddPCR can be successfully employed to detect rare mutations in microbial genomes (Morella et al., 2018).

Moreover, here established droplet-based methodology could be utilized to understand ecological and (co)evolutionary aspects of dynamics between bacteria and their phages, especially bacteria-phage dynamics at low bacterial population densities (van Houte et al., 2016; Koskella et al., 2022). For instance, stable long-term time-lapse imaging of droplet-environments at a specific temperature could provide the optimal platform for investigating interactions between temperate phages and their bacterial hosts. Temperate phages, in addition to their lytic cycle, can also display a lysogenic life cycle by integrating their genome into the genome of their host. Droplet assays could help apprehend dynamics of switching from lysogenic to lytic cycle and vice versa, and provide insights into how this switch changes structure and behavior of the bacterial host population. In particular, the peptide signal-mediated short-range communication between phages, which controls lysogeny-lysis decision based on the bacterial host densities (Erez et al., 2017; Aframian et al., 2022), could be monitored in droplet-environments.

In addition to capturing quorum sensing molecules and secreted proteins, droplet-environments can allow bacterial cells to maintain native planktonic and aggregate lifestyles and form biofilms (Chang et al., 2015). The aggregate formation can be induced by various stressors, occurring even as a response to phage infection, and can generally render bacterial pathogens resilient to the immune system and antimicrobial treatments (Trunk et al., 2018; Cai, 2020; Cai et al., 2022). Recent time-lapse microscopy studies of bacteria-phage dynamics employed microfluidic devices with confined habitats (so called mother machines), which support one-dimensional growth of bacterial cells preventing them from forming aggregates or biofilms (Attrill et al., 2021; Nikolic et al., 2023). Our experiments showed that aggregates can be formed from single bacterial cells within a droplet (Supplementary Movie S1), thus enabling us to evaluate phage efficacy against individual cells as well as aggregates within the population.

Extension of the method to screening a larger number of droplets will provide more insights into stochastic processes at play when bacterial populations start growing from just few cells (Barizien et al., 2019). This could be done by designing devices with more traps in the field of view. With more droplet assays per time-lapse experiment, rare events corresponding to emergence of bacterial resistance (genetic basis) and tolerance (non-genetic basis) to phages could also be identified, and resilient bacteria extracted from the chip to determine the underlying mechanisms that shape bacterial antiphage defense strategies. In addition to bacterial strains that have chromosomally encoded or plasmid-based fluorescent gene reporters, our setup could be employed to analyze bacterial cultures of any strain stained with fluorescent dyes prior to phage infection (Yoon et al., 2021). Moreover, future work could utilize fluorescent dyes to label phages outside host cells (Egido et al., 2023), to apprehend dynamics of both bacteria and phage numbers over time, and better understand the progression of phage infection. Finally, alternative single-cell methodologies that do not require bacteria to be fluorescently-labeled, would be useful to detect growth and phage-induced lysis of individual bacterial cells from brightfield microscopy images using deep

learning-based algorithms (Howell et al., 2022; Tiwari et al., 2023). To conclude, the development of novel population-level and single-cell tools and approaches will expedite research towards understanding what makes phages effective bacteria-killers and how their bacterial hosts can eventually mitigate phage invasion, highlighting the best phage candidates for phage therapy against specific bacterial diseases.

Data availability statement

The original contributions presented in the study are included in the article/Supplementary material, further inquiries can be directed to the corresponding authors. Design files for microfluidic devices are deposited on DropBase (https://openwetware.org/wiki/DropBase:Anchored_droplet).

Author contributions

NN: Conceptualization, Data curation, Formal analysis, Funding acquisition, Investigation, Methodology, Supervision, Validation, Visualization, Writing – original draft, Writing – review & editing. VA: Methodology, Resources, Writing – review & editing. AT: Methodology, Visualization, Writing – review & editing. RC: Funding acquisition, Methodology, Resources, Validation, Writing – review & editing. FG: Conceptualization, Data curation, Funding acquisition, Methodology, Project administration, Resources, Supervision, Writing – original draft, Writing – review & editing.

Funding

The author(s) declare financial support was received for the research, authorship, and/or publication of this article. This work was supported by the BBSRC grant BB/T011777/1 to FG, by the Wellcome Trust Institutional Strategic Support Funding (WT105618MA) Research Restart Award and Pump-Priming Initiative to NN, by the Royal Society grant RGS/R2/192377 to RC, and by the BBSRC-funded South West Biosciences Doctoral Training Partnership (training grant reference 2578821).

Acknowledgments

The authors thank Lucy Witherall and Wolfram Möbius for sharing the phage T7 lysate and strain BW25113, and for their technical support, Tobias Bergmiller for sharing bacterial strains, and Lisa Butt and Ivana Gudelj for sharing equipment. The authors acknowledge the LSI Technical Services Team at the University of Exeter and use of the Exeter Microfluidics Facility and Savchenko Centre for Nanoscience.

Conflict of interest

The authors declare that the research was conducted in the absence of any commercial or financial relationships that could be construed as a potential conflict of interest.

Publisher's note

All claims expressed in this article are solely those of the authors and do not necessarily represent those of their affiliated organizations, or those of the publisher, the editors and the reviewers. Any product that may be evaluated in this article, or claim that may be made by its manufacturer, is not guaranteed or endorsed by the publisher.

Supplementary material

The Supplementary material for this article can be found online at: <https://www.frontiersin.org/articles/10.3389/fmicb.2023.1260196/full#supplementary-material>

References

- Abedon, S. T. (2019). Use of phage therapy to treat long-standing, persistent, or chronic bacterial infections. *Adv. Drug Deliv. Rev.* 145, 18–39. doi: 10.1016/j.addr.2018.06.018
- Abedon, S. T., Danis-Wlodarczyk, K. M., and Alves, D. R. (2021). Phage therapy in the 21st century: is there modern, clinical evidence of phage-mediated efficacy? *Pharmaceuticals* 14:1157. doi: 10.3390/ph14111157
- Ács, N., Gambino, M., and Brøndsted, L. (2020). Bacteriophage enumeration and detection methods. *Front. Microbiol.* 11:594868. doi: 10.3389/fmicb.2020.594868
- Aframian, N., Omer Bendori, S., Kabel, S., Guler, P., Stokar-Avihail, A., Manor, E., et al. (2022). Dormant phages communicate via arbitrium to control exit from lysogeny. *Nat. Microbiol.* 7, 145–153. doi: 10.1038/s41564-021-01008-5
- Allocati, N., Masulli, M., Alexeyev, M. F., and Di Ilio, C. (2013). *Escherichia coli* in Europe: an overview. *Int. J. Environ. Res. Public Health* 10, 6235–6254. doi: 10.3390/ijerph10126235
- Anagnostidis, V., Sherlock, B., Metz, J., Mair, P., Hollfelder, F., and Gielen, F. (2020). Deep learning guided image-based droplet sorting for on-demand selection and analysis of single cells and 3D cell cultures. *Lab Chip* 20, 889–900. doi: 10.1039/D0LC00055H
- Atrill, E. L., Claydon, R., Łapińska, U., Recker, M., Meaden, S., Brown, A. T., et al. (2021). Individual bacteria in structured environments rely on phenotypic resistance to phage. *PLoS Biol.* 19:e3001406. doi: 10.1371/journal.pbio.3001406
- Barizien, A., Suryateja Jammalamadaka, M. S., Amselem, G., and Baroud, C. N. (2019). Growing from a few cells: combined effects of initial stochasticity and cell-to-cell variability. *J. R. Soc. Interface* 16:20180935. doi: 10.1098/rsif.2018.0935
- Bentley, S. A., Laeverenz-Schlogelhofer, H., Anagnostidis, V., Cammann, J., Mazza, M. G., Gielen, F., et al. (2022). Phenotyping single-cell motility in microfluidic confinement. *eLife* 11:e76519. doi: 10.7554/eLife.76519
- Bernhardt, T. G., Wang, N., Struck, D. K., and Young, R. (2002). Breaking free: “protein antibiotics” and phage lysis. *Res. Microbiol.* 153, 493–501. doi: 10.1016/S0923-2508(02)01330-X
- Bonten, M., Johnson, J. R., van den Biggelaar, A. H., Georgalis, L., Geurtsen, J., de Palacios, P. I., et al. (2021). Epidemiology of *Escherichia coli* bacteremia: a systematic literature review. *Clin. Infect. Dis.* 72, 1211–1219. doi: 10.1093/cid/ciaa210
- Cai, Y. M. (2020). Non-surface attached bacterial aggregates: a ubiquitous third lifestyle. *Front. Microbiol.* 11:557035. doi: 10.3389/fmicb.2020.557035
- Cai, Y. M., Yu, K. W., Liu, J. H., Cai, Z., Zhou, Z. H., Liu, Y., et al. (2022). The c-di-GMP phosphodiesterase PipA (PA0285) regulates autoaggregation and Pf4 bacteriophage production in *Pseudomonas aeruginosa* PAO1. *Appl. Environ. Microbiol.* 88, e00039–e00022. doi: 10.1128/aem.00039-22
- Chait, R., Ruess, J., Bergmiller, T., Tkačik, G., and Guet, C. C. (2017). Shaping bacterial population behavior through computer-interfaced control of individual cells. *Nat. Commun.* 8:1535. doi: 10.1038/s41467-017-01683-1
- Champagne-Jorgensen, K., Luong, T., Darby, T., and Roach, D. R. (2023). Immunogenicity of bacteriophages. *Trends Microbiol.* 31, 1058–1071. doi: 10.1016/j.tim.2023.04.008
- Chang, C. B., Wilking, J. N., Kim, S. H., Shum, H. C., and Weitz, D. A. (2015). Monodisperse emulsion drop microenvironments for bacterial biofilm growth. *Small* 11, 3954–3961. doi: 10.1002/smll.201403125
- Chory, E. J., Grettton, D. W., DeBenedictis, E. A., and Esvelt, K. M. (2021). Enabling high-throughput biology with flexible open-source automation. *Mol. Syst. Biol.* 17:e9942. doi: 10.15252/msb.20209942
- Cohen, D. E., Schneider, T., Wang, M., and Chiu, D. T. (2010). Self-digitization of sample volumes. *Anal. Chem.* 82, 5707–5717. doi: 10.1021/ac100713u
- Collins, D. J., Neild, A., DeMello, A., Liu, A. Q., and Ai, Y. (2015). The Poisson distribution and beyond: methods for microfluidic droplet production and single cell encapsulation. *Lab Chip* 15, 3439–3459. doi: 10.1039/C5LC00614G
- Dedrick, R. M., Guerrero-Bustamante, C. A., Garlena, R. A., Russell, D. A., Ford, K., Harris, K., et al. (2019). Engineered bacteriophages for treatment of a patient with a disseminated drug-resistant *Mycobacterium abscessus*. *Nat. Med.* 25, 730–733. doi: 10.1038/s41591-019-0437-z
- Edelstein, A. D., Tsuchida, M. A., Amodaj, N., Pinkard, H., Vale, R. D., and Stuurman, N. (2014). Advanced methods of microscope control using µManager software. *J. Biol. Methods* 1:e10. doi: 10.14440/jbm.2014.36
- Egido, J. E., Toner-Bartelds, C., Costa, A. R., Brouns, S. J., Rooijackers, S. H., Bardoel, B. W., et al. (2023). Monitoring phage-induced lysis of gram-negatives in real time using a fluorescent DNA dye. *Sci. Rep.* 13:856. doi: 10.1038/s41598-023-27734-w
- Erez, Z., Steinberger-Levy, I., Shamir, M., Doron, S., Stokar-Avihail, A., Peleg, Y., et al. (2017). Communication between viruses guides lysis-lysogeny decisions. *Nature* 541, 488–493. doi: 10.1038/nature21049
- Gantz, M., Neun, S., Medcalf, E. J., van Vliet, L. D., and Hollfelder, F. (2023). Ultrahigh-throughput enzyme engineering and discovery in *in vitro* compartments. *Chem. Rev.* 123, 5571–5611. doi: 10.1021/acs.chemrev.2c00910
- Gibson, S. B., Green, S. I., Liu, C. G., Salazar, K. C., Clark, J. R., Terwilliger, A. L., et al. (2019). Constructing and characterizing bacteriophage libraries for phage therapy of human infections. *Front. Microbiol.* 10:2537. doi: 10.3389/fmicb.2019.02537
- Gielen, F., Colin, P. Y., Mair, P., and Hollfelder, F. (2018). “Ultrahigh-throughput screening of single-cell lysates for directed evolution and functional metagenomics” in *Protein engineering: methods and protocols* (New York, NY: Humana Press), 297–309.
- Gielen, F., Hours, R., Emond, S., Fischlechner, M., Schell, U., and Hollfelder, F. (2016). Ultrahigh-throughput-directed enzyme evolution by absorbance-activated droplet sorting (AADS). *Proc. Natl. Acad. Sci. U.S.A.* 113, E7383–E7389. doi: 10.1073/pnas.1606927113
- Henn, M. R., Sullivan, M. B., Stange-Thomann, N., Osburne, M. S., Berlin, A. M., Kelly, L., et al. (2010). Analysis of high-throughput sequencing and annotation strategies for phage genomes. *PLoS One* 5:e9083. doi: 10.1371/journal.pone.0009083
- Howell, L., Anagnostidis, V., and Gielen, F. (2022). Multi-object detector yolov4-tiny enables high-throughput combinatorial and spatially-resolved sorting of cells in microdroplets. *Adv. Mater. Technol.* 7:2101053. doi: 10.1002/admt.202101053
- Hsu, R. H., Clark, R. L., Tan, J. W., Ahn, J. C., Gupta, S., Romero, P. A., et al. (2019). Microbial interaction network inference in microfluidic droplets. *Cell Syst.* 9, 229–242.e4. doi: 10.1016/j.cels.2019.06.008
- Huang, S., Srimani, J. K., Lee, A. J., Zhang, Y., Lopatkin, A. J., Leong, K. W., et al. (2015). Dynamic control and quantification of bacterial population dynamics in droplets. *Biomaterials* 61, 239–245. doi: 10.1016/j.biomaterials.2015.05.038
- Igler, C. (2022). Phenotypic flux: the role of physiology in explaining the conundrum of bacterial persistence amid phage attack. *Virus Evol.* 8:veac086. doi: 10.1093/ve/veac086
- Ikuta, K. S., Swetschinski, L. R., Aguilar, G. R., Sharara, F., Mestrovic, T., Gray, A. P., et al. (2022). Global mortality associated with 33 bacterial pathogens in 2019: a systematic analysis for the global burden of disease study 2019. *Lancet* 400, 2221–2248. doi: 10.1016/S0140-6736(22)02185-7
- Jack, B. R., Boutz, D. R., Paff, M. L., Smith, B. L., and Wilke, C. O. (2019). Transcript degradation and codon usage regulate gene expression in a lytic phage. *Virus Evol.* 5:vez055. doi: 10.1093/ve/vez055

- Jenkins, S. T., Beard, J. P., and Howe, T. G. (1974). Male-specific bacteriophage MS2 propagation in fluorophenylalanine-resistant *Escherichia coli* K12. *J. Virol.* 14, 50–55. doi: 10.1128/jvi.14.1.50-55.1974
- Kaushik, A. M., Hsieh, K., Chen, L., Shin, D. J., Liao, J. C., and Wang, T. H. (2017). Accelerating bacterial growth detection and antimicrobial susceptibility assessment in integrated picoliter droplet platform. *Biosens. Bioelectron.* 97, 260–266. doi: 10.1016/j.bios.2017.06.006
- Klein, R. D., and Hultgren, S. J. (2020). Urinary tract infections: microbial pathogenesis, host–pathogen interactions and new treatment strategies. *Nat. Rev. Microbiol.* 18, 211–226. doi: 10.1038/s41579-020-0324-0
- Kleine-Brüggeny, H., Van Vliet, L. D., Mulas, C., Gielen, F., Agle, C. C., Silva, J. C., et al. (2019). Long-term perfusion culture of monoclonal embryonic stem cells in 3D hydrogel beads for continuous optical analysis of differentiation. *Small* 15:e1804576. doi: 10.1002/sml.201804576
- Kortright, K. E., Chan, B. K., Koff, J. L., and Turner, P. E. (2019). Phage therapy: a renewed approach to combat antibiotic-resistant bacteria. *Cell Host Microbe* 25, 219–232. doi: 10.1016/j.chom.2019.01.014
- Koskella, B., Hernandez, C. A., and Wheatley, R. M. (2022). Understanding the impacts of bacteriophage viruses: from laboratory evolution to natural ecosystems. *Annu. Rev. Virol.* 9, 57–78. doi: 10.1146/annurev-virology-091919-075914
- Lefkowitz, E. J., Dempsey, D. M., Hendrickson, R. C., Orton, R. J., Siddell, S. G., and Smith, D. B. (2017). Virus taxonomy: the database of the international committee on taxonomy of viruses (ICTV). *Nucleic Acids Res.* 46, D708–D717. doi: 10.1093/nar/gkx932
- Leung, K., Zahn, H., Leaver, T., Konwar, K. M., Hanson, N. W., Pagé, A. P., et al. (2012). A programmable droplet-based microfluidic device applied to multiparameter analysis of single microbes and microbial communities. *Proc. Natl. Acad. Sci. U.S.A.* 109, 7665–7670. doi: 10.1073/pnas.1106752109
- Liu, X., Painter, R. E., Enesa, K., Holmes, D., Whyte, G., Garlisi, C. G., et al. (2016). High-throughput screening of antibiotic-resistant bacteria in picodroplets. *Lab Chip* 16, 1636–1643. doi: 10.1039/C6LC00180G
- Maffei, E., Shaidullina, A., Burkolter, M., Heyer, Y., Estermann, F., Druelle, V., et al. (2021). Systematic exploration of *Escherichia coli* phage-host interactions with the BASEL phage collection. *PLoS Biol.* 19:e3001424. doi: 10.1371/journal.pbio.3001424
- Mahler, L., Wink, K., Beulig, R. J., Scherlach, K., Tovar, M., Zang, E., et al. (2018). Detection of antibiotics synthesized in microfluidic picolitre-droplets by various actinobacteria. *Sci. Rep.* 8:13087. doi: 10.1038/s41598-018-31263-2
- Maimaiti, Z., Li, Z., Xu, C., Chen, J., and Chai, W. (2023). Global trends and hotspots of phage therapy for bacterial infection: a bibliometric visualized analysis from 2001 to 2021. *Front. Microbiol.* 13:13:1067803. doi: 10.3389/fmicb.2022.1067803
- Matula, K., Rivello, F., and Huck, W. T. (2020). Single-cell analysis using droplet microfluidics. *Adv. Biosyst.* 4:1900188. doi: 10.1002/adbi.201900188
- McCallin, S., Sacher, J. C., Zheng, J., and Chan, B. K. (2019). Current state of compassionate phage therapy. *Viruses* 11:343. doi: 10.3390/v11040343
- McCowan, C., Bakshi, A., McConnachie, A., Malcolm, W., Barry, S. J., Santiago, V. H., et al. (2022). Coli bacteraemia and antimicrobial resistance following antimicrobial prescribing for urinary tract infection in the community. *BMC Infect. Dis.* 22:805. doi: 10.1186/s12879-022-07768-7
- Model, M. A., and Burkhardt, J. K. (2001). A standard for calibration and shading correction of a fluorescence microscope. *Cytometry* 44, 309–316. doi: 10.1002/1097-0320(20010801)44:4<309::AID-CYTO1122>3.0.CO;2-3
- Morella, N. M., Yang, S. C., Hernandez, C. A., and Koskella, B. (2018). Rapid quantification of bacteriophages and their bacterial hosts *in vitro* and *in vivo* using droplet digital PCR. *J. Virol. Methods* 259, 18–24. doi: 10.1016/j.jviromet.2018.05.007
- Mühlen, S., and Dersch, P. (2020). Treatment strategies for infections with Shiga toxin-producing *Escherichia coli*. *Front. Cell. Infect. Microbiol.* 10:16. doi: 10.3389/fcimb.2020.00169
- Murray, C. J., Ikuta, K. S., Sharara, F., Swetschinski, L., Aguilar, G. R., Gray, A., et al. (2022). Global burden of bacterial antimicrobial resistance in 2019: a systematic analysis. *Lancet* 399, 629–655. doi: 10.1016/S0140-6736(21)02724-0
- Nale, J. Y., and Clokie, M. R. (2021). Preclinical data and safety assessment of phage therapy in humans. *Curr. Opin. Biotechnol.* 68, 310–317. doi: 10.1016/j.copbio.2021.03.002
- Nguyen, H. M., and Kang, C. (2014). Lysis delay and burst shrinkage of coliphage T7 by deletion of terminator T ϕ reversed by deletion of early genes. *J. Virol.* 88, 2107–2115. doi: 10.1128/JVI.03274-13
- Nikolic, N., Bergmiller, T., Pleska, M., and Guet, C. C. Bacterial toxin-antitoxin system MazEF as a native defense mechanism against RNA phages in *Escherichia coli*. *bioRxiv* (2023) Available at: <https://doi.org/10.1101/2023.02.01.526697> [Epub ahead of preprint].
- Petrovic Fabijan, A., Iredell, J., Danis-Wlodarczyk, K., Kebriaei, R., and Abedon, S. T. (2023). Translating phage therapy into the clinic: recent accomplishments but continuing challenges. *PLoS Biol.* 21:e3002119. doi: 10.1371/journal.pbio.3002119
- Postek, W., Gargulinski, P., Scheler, O., Kaminski, T. S., and Garstecki, P. (2018). Microfluidic screening of antibiotic susceptibility at a single-cell level shows the inoculum effect of cefotaxime on *E. coli*. *Lab Chip* 18, 3668–3677. doi: 10.1039/C8LC00916C
- Pratt, S. L., Zath, G. K., Akiyama, T., Williamson, K. S., Franklin, M. J., and Chang, C. B. (2019). DropSOAC: stabilizing microfluidic drops for time-lapse quantification of single-cell bacterial physiology. *Front. Microbiol.* 10:2112. doi: 10.3389/fmicb.2019.02112
- Rappaport, I. (1965). Some studies of the infectious process with MS2 bacteriophage. *Biochim. Biophys. Acta* 103, 486–494. doi: 10.1016/0005-2787(65)90141-3
- Rutkauskaite, J., Berger, S., Stavrakis, S., Dressler, O., Heyman, J., Casadevall I Solvas, X., et al. (2022). High-throughput single-cell antibody secretion quantification and enrichment using droplet microfluidics-based FRET assay. *iScience* 25:104515. doi: 10.1016/j.isci.2022.104515
- Sabbachandani, P., Sarkar, S., Zucchi, P. C., Whitfield, B. A., Kirby, J. E., Hirsch, E. B., et al. (2017). Integrated microfluidic platform for rapid antimicrobial susceptibility testing and bacterial growth analysis using bead-based biosensor via fluorescence imaging. *Microchim. Acta* 184, 4619–4628. doi: 10.1007/s00604-017-2492-9
- Schindelin, J., Arganda-Carreras, I., Frise, E., Kaynig, V., Longair, M., Pietzsch, T., et al. (2012). Fiji: an open-source platform for biological-image analysis. *Nat. Methods* 9, 676–682. doi: 10.1038/nmeth.2019
- Spilsberg, B., Sekse, C., Urdahl, A. M., Nesse, L. L., and Johannessen, G. S. (2021). Persistence of a Stx-encoding bacteriophage in minced meat investigated by application of an improved DNA extraction method and digital droplet PCR. *Front. Microbiol.* 11:581575. doi: 10.3389/fmicb.2020.581575
- Strathdee, S. A., Hatfull, G. F., Mutalik, V. K., and Schooley, R. T. (2023). Phage therapy: from biological mechanisms to future directions. *Cells* 186, 17–31. doi: 10.1016/j.cell.2022.11.017
- Suh, G. A., Lodise, T. P., Tamma, P. D., Knisely, J. M., Alexander, J., Aslam, S., et al. (2022). Considerations for the use of phage therapy in clinical practice. *Antimicrob. Agents Chemother.* 66, e02071–e02021. doi: 10.1128/aac.02071-21
- Sun, H., Xie, W., Mo, J., Huang, Y., and Dong, H. (2023). Deep learning with microfluidics for on-chip droplet generation, control, and analysis. *Front. Bioeng. Biotechnol.* 11:1208648. doi: 10.3389/fbioe.2023.1208648
- Taylor, D., Verdon, N., Lomax, P., Allen, R. J., and Titmuss, S. (2022). Tracking the stochastic growth of bacterial populations in microfluidic droplets. *Phys. Biol.* 19:026003. doi: 10.1088/1478-3975/ac4c9b
- Tiwari, A., Nikolic, N., Anagnostidis, V., and Gielen, F. (2023). Label-free analysis of bacterial growth and lysis at the single-cell level using droplet microfluidics and object detection-oriented deep learning. *Front. Lab. Chip. Technol.* 2. doi: 10.3389/frlct.2023.1258155
- Tjhung, K. F., Burnham, S., Anany, H., Griffiths, M. W., and Derda, R. (2014). Rapid enumeration of phage in monodisperse emulsions. *Anal. Chem.* 86, 5642–5648. doi: 10.1021/ac500244g
- Trunk, T., Khalil, H. S., and Leo, J. C. (2018). Bacterial autoaggregation. *AIMS Microbiol.* 4, 140–164. doi: 10.3934/microbiol.2018.1.140
- Tsukada, K., Okazaki, M., Kita, H., Inokuchi, Y., Urabe, I., and Yomo, T. (2009). Quantitative analysis of the bacteriophage Q β infection cycle. *Biochim. Biophys. Acta* 1790, 65–70. doi: 10.1016/j.bbagen.2008.08.007
- UK Health Security Agency. *English surveillance programme for antimicrobial utilisation and resistance (ESPAUR) report 2021 to 2022*. London: UK Health Security Agency, (2022).
- van Duin, J., and Tsareva, N. (2006) in *Single-stranded RNA phages*. ed. R. L. Calendar (Oxford: Oxford University Press), 175–196.
- van Houte, S., Buckling, A., and Westra, E. R. (2016). Evolutionary ecology of prokaryotic immune mechanisms. *Microbiol. Mol. Biol. Rev.* 80, 745–763. doi: 10.1128/MMBR.00011-16
- Van Nieuwenhuysse, B., Van der Linden, D., Chatzis, O., Lood, C., Wagemans, J., Lavigne, R., et al. (2022). Bacteriophage-antibiotic combination therapy against extensively drug-resistant *Pseudomonas aeruginosa* infection to allow liver transplantation in a toddler. *Nat. Commun.* 13:5725. doi: 10.1038/s41467-022-33294-w
- Venturini, C., Petrovic Fabijan, A., Fajardo Lubian, A., Barbirz, S., and Iredell, J. (2022). Biological foundations of successful bacteriophage therapy. *EMBO Mol. Med.* 14:e12435. doi: 10.15252/emmm.202012435
- Walker, P. J., Siddell, S. G., Lefkowitz, E. J., Mushegian, A. R., Adriaenssens, E. M., Alfenas-Zerbini, P., et al. (2022). Recent changes to virus taxonomy ratified by the International Committee on Taxonomy of Viruses (2022). *Arch. Virol.* 167, 2429–2440. doi: 10.1007/s00705-022-05516-5
- WHO (2019). “No time to wait: Securing the future from drug-resistant infections” in *Report to the secretary-general of the United Nations* (Geneva, Switzerland: WHO)
- Woody, M. A., and Cliver, D. O. (1995). Effects of temperature and host cell growth phase on replication of F-specific RNA coliphage QBeta. *Appl. Environ. Microbiol.* 61, 1520–1526. doi: 10.1128/aem.61.4.1520-1526.1995
- Xu, H., Bao, X., Hong, W., Wang, A., Wang, K., Dong, H., et al. (2021). Biological characterization and evolution of bacteriophage T7- Δ holin during the serial passage process. *Front. Microbiol.* 12:705310. doi: 10.3389/fmicb.2021.705310
- Xu, X., Wang, J., Wu, L., Guo, J., Song, Y., Tian, T., et al. (2020). Microfluidic single-cell omics analysis. *Small* 16:1903905. doi: 10.1002/sml.201903905

Yang, Y., Shen, W., Zhong, Q., Chen, Q., He, X., Baker, J. L., et al. (2020). Development of a bacteriophage cocktail to constrain the emergence of phage-resistant *Pseudomonas aeruginosa*. *Front. Microbiol.* 11:327. doi: 10.3389/fmicb.2020.00327

Yoon, S. A., Park, S. Y., Cha, Y., Gopala, L., and Lee, M. H. (2021). Strategies of detecting bacteria using fluorescence-based dyes. *Front. Chem.* 9:743923. doi: 10.3389/fchem.2021.743923

Yu, J. Q., Huang, W., Chin, L. K., Lei, L., Lin, Z. P., Ser, W., et al. (2014). Droplet optofluidic imaging for λ -bacteriophage detection via co-culture with host cell *Escherichia coli*. *Lab Chip* 14, 3519–3524. doi: 10.1039/C4LC00042K

Zrelavs, N., Dislers, A., and Kazaks, A. (2020). Motley crew: overview of the currently available phage diversity. *Front. Microbiol.* 11:579452. doi: 10.3389/fmicb.2020.579452